Supplementary Information for A Threefold Increase in Observed Summertime Atmospheric Dimethyl Sulfide over the Austral Southern Ocean

Caleb Mynard[1*], Megan D. Willis[2], Nigel Somerville[3], Alan Griffiths[4], Sally Taylor[1], Greg P. Ayers[5], Melita Keywood[1], Erin Dunne[1], Emily B. Franklin[1*]

[1]CSIRO Environment, Aspendale, VIC, Australia.
[2]Department of Chemistry, Colorado State University, Fort Collins, CO, USA.
[3]Bureau of Meteorology, Smithton, TAS, Australia.
[4]Australian Nuclear Science and Technology Organisation, Lucas Heights, NSW, Australia.
[5]Ayers Advisory Pty Ltd, Melbourne, VIC, Australia.

*Corresponding author(s). E-mail(s): caleb.mynard@csiro.au; emily.franklin@csiro.au;

1 Contents of this file

Season	1993-1996	2023-2026
Summer (DJF)	61 ± 41 (BDL–368)	180 ± 103 (46–915)
Autumn (MAM)	32 ± 25 (BDL–269)	51 ± 22 (8–121)
Winter (JJA)	9 ± 6 (BDL–103)	34 ± 14 (BDL–76)
Spring (SON)	18 ± 20 (BDL–143)	50 ± 30 (8–305)

Table S1 Seasonal mean atmospheric DMS concentrations (mean ± standard deviation of 30-min data) are shown for the 1993–1996 [1] and 2023–2026 (this study) periods. Values in parentheses indicate the observed range for each season, with BDL denoting measurements below the detection limit.

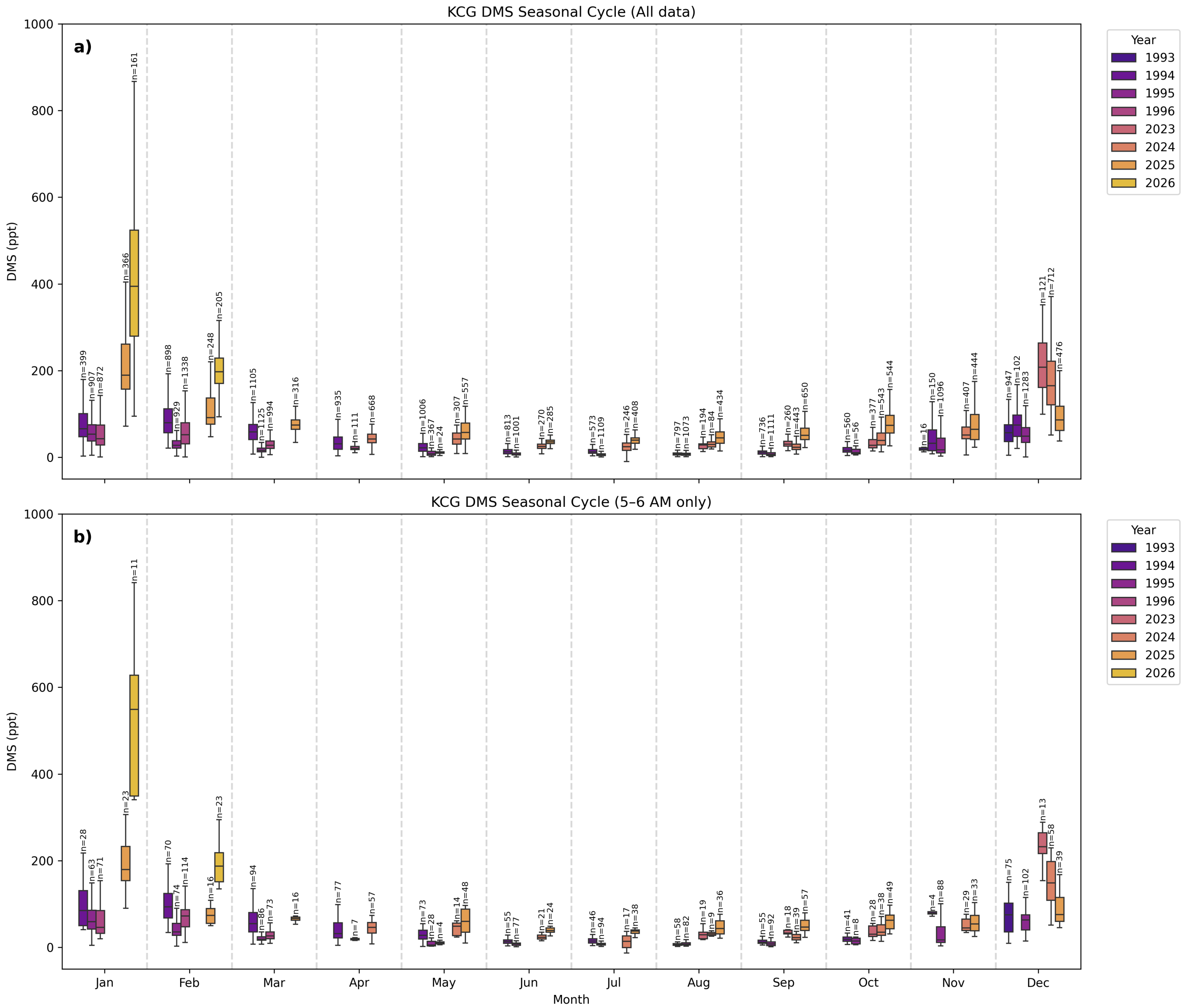

Fig. S1 Seasonal cycle of atmospheric dimethyl sulfide (DMS) concentrations at KCG under full and restricted diurnal sampling conditions. (a) Monthly distributions of DMS (ppt) for the full dataset, combining all available observations from the Gillet (1990s) and Mynard (2020s) periods. (b) As in (a), but restricted to early-morning observations (05:00–06:00 local time) to isolate a consistent diurnal window and reduce the influence of diel variability. Boxplots show the interquartile range (IQR) with medians, whiskers extending to 1.5×IQR, and individual year-specific distributions separated by hue. Sample sizes (n) are annotated for each month–year combination.

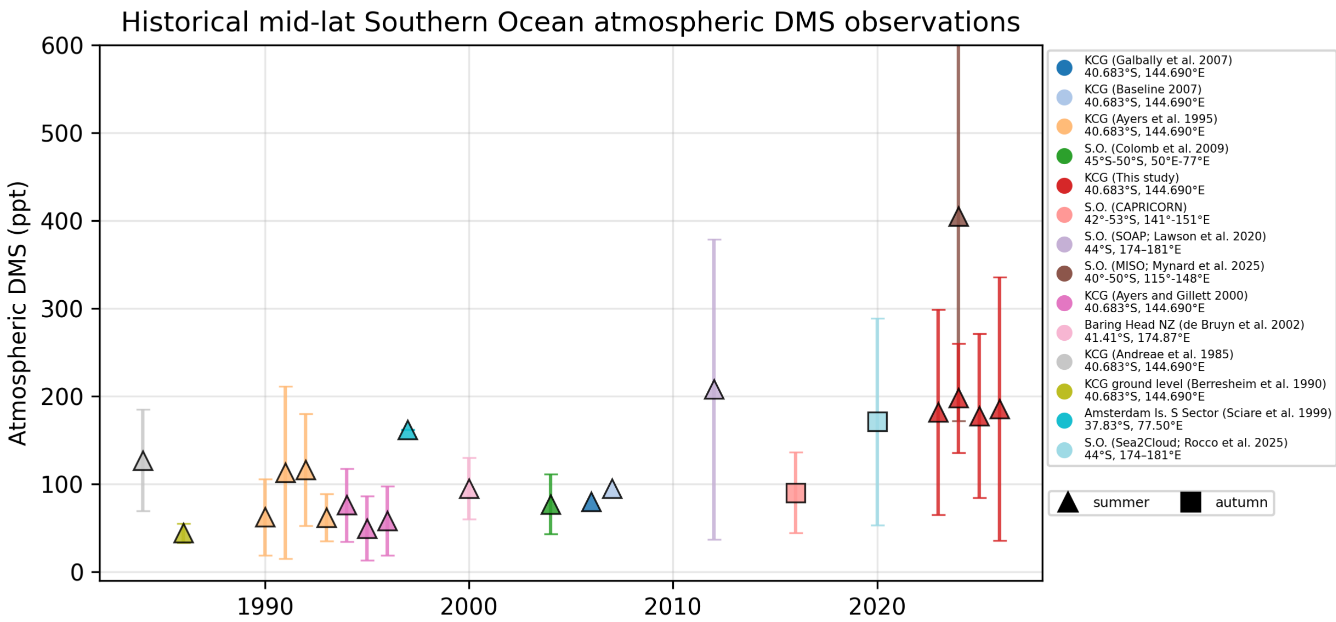

Fig. S2 Historical observations of yearly (DJF months) or campaign mean atmospheric DMS in the mid-latitude Southern Ocean (∼40–50° S). Reported atmospheric DMS concentrations from published observations are shown by year, with colours corresponding to individual studies. Error bars indicate the reported standard deviation. Marker shapes denote season, with triangles representing summer and squares representing autumn. References for each individual study are included in the References section below.

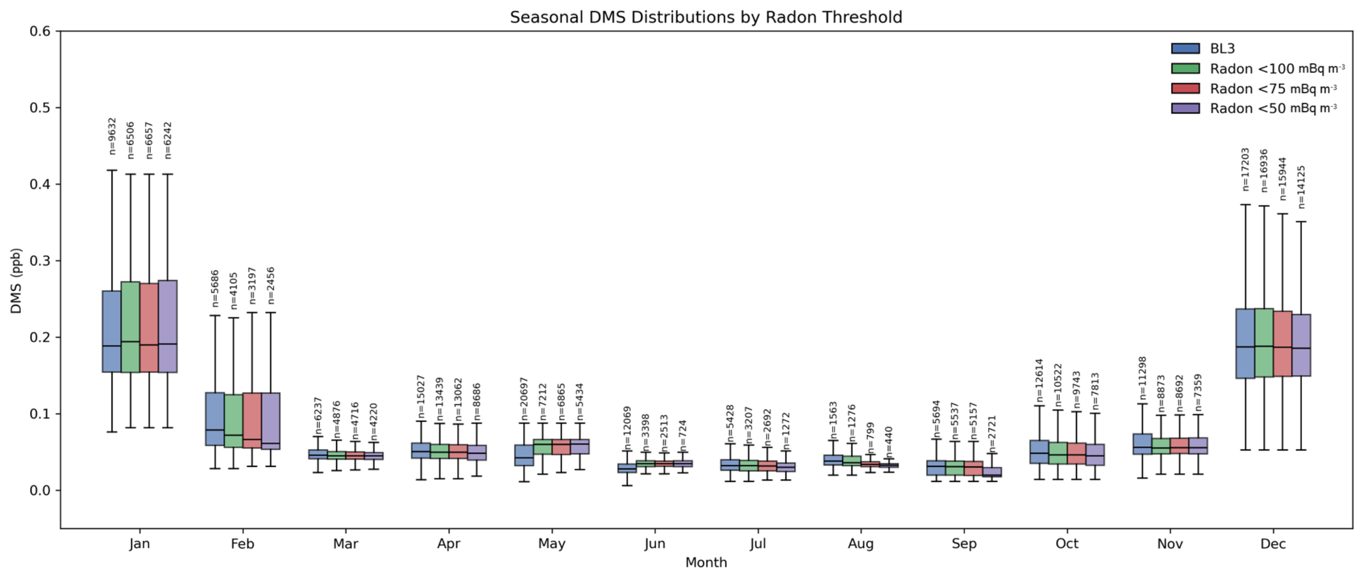

Fig. S3 Seasonal cycle (April 2024–April 2025) DMS distributions over radon thresholds. BL3 (blue) is based on a baseline flag from measured wind direction occurring within the Southern Ocean baseline sector (190–280°), which is similar to the Southern Ocean air mass filtering by Ayers and Gillett [1]. Radon thresholds are derived from 30-min measurements: <100 mBq m^{-3} (green), <75 mBq m^{-3} (red) and <50 mBq m^{-3} (purple).

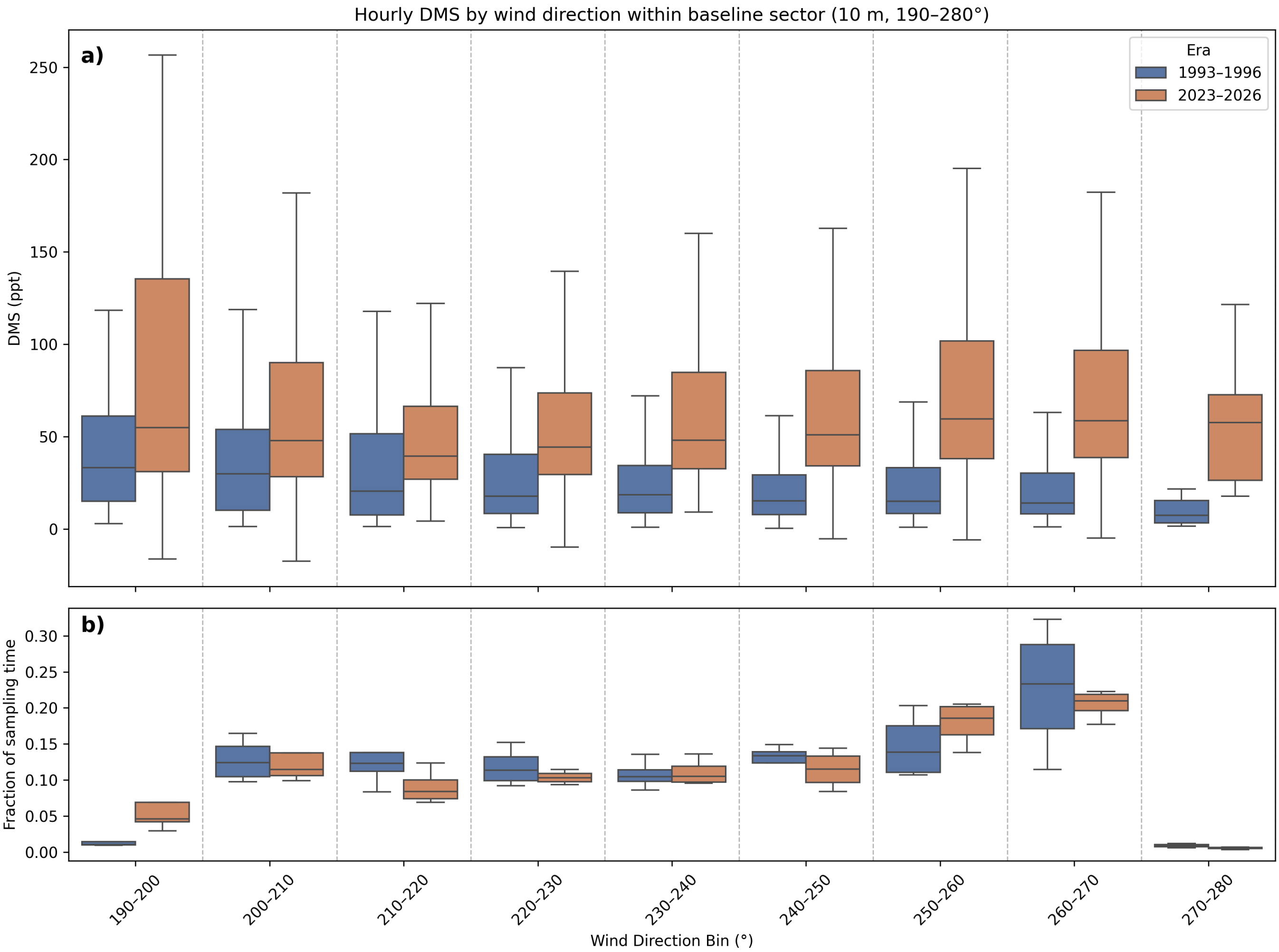

Fig. S4 Southern Ocean ("Baseline") wind sector (190°–280°) analysis comparing the 1993–1996 (blue) and 2023–2026 (orange) observation periods. (a) Hourly DMS concentrations (ppt) across 10° wind direction bins. (b) The relative fraction of sampling time per year distributed across each wind bin. Boxplots show medians and IQRs; extreme outliers are excluded from display.

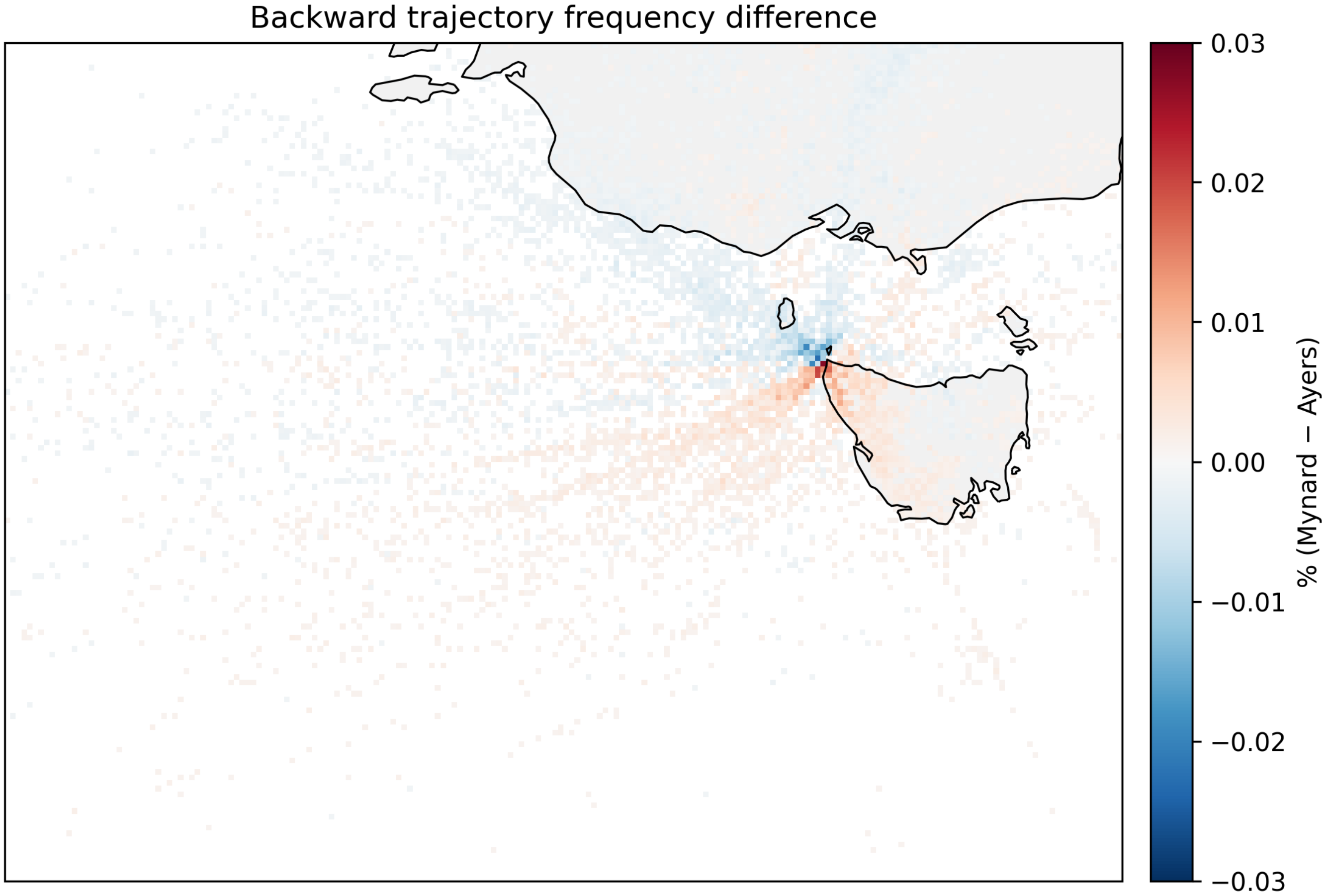

Fig. S5 Difference in normalised 48-h back-trajectory residence frequency (% of total trajectory points) between this study (2023-2026) and Ayers and Gillet (2000) 1993-1996 periods, shown on a 0.1° × 0.1° latitude–longitude grid (Mynard - Ayers)

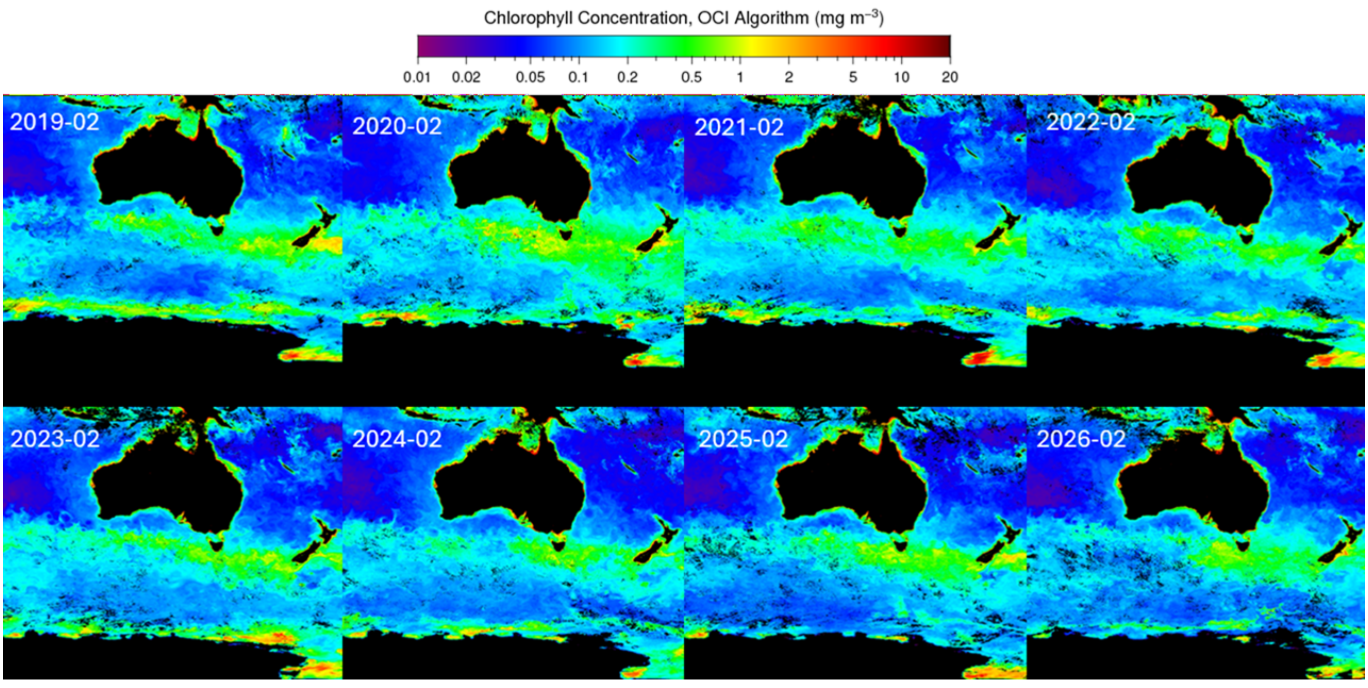

Fig. S6 Monthly MODIS chlorophyll-a retrievals [14] of the month of February from 2019 to 2026 over the Australiasian Southern Ocean sector.

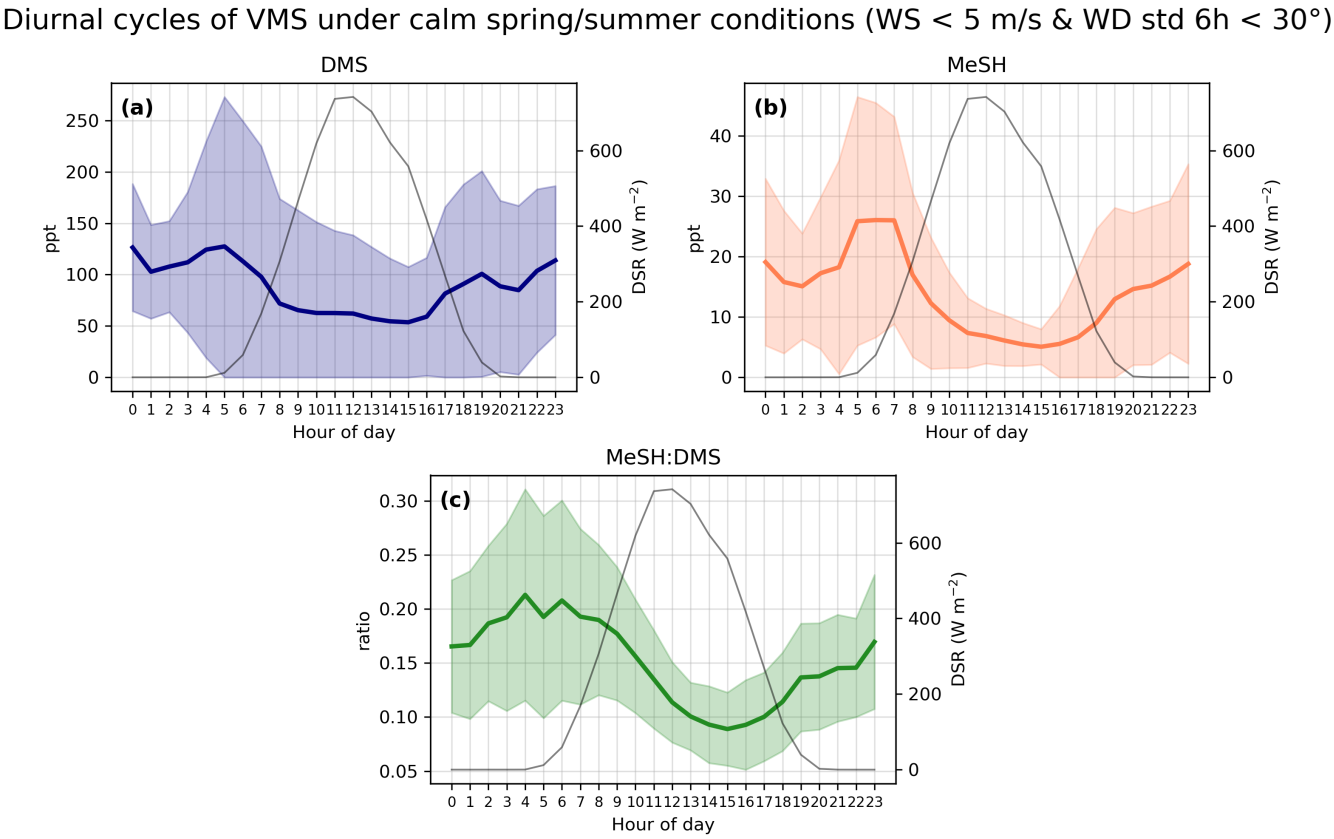

Fig. S7 Diurnal cycles of (a) DMS, (b) MeSH, and (c) MeSH:DMS under defined calm conditions in all spring-summer hourly data (33 equivalent days): in-situ wind speed <5 ms^{-1} and 6 hour circular standard deviation of in-situ wind direction <30°. Highlighted regions are the 25-75th percentiles. The grey line is the in-situ measured median downwelling shortwave radiation (DSR) at KCGBAPS. The hour of day is in local time (AEST).

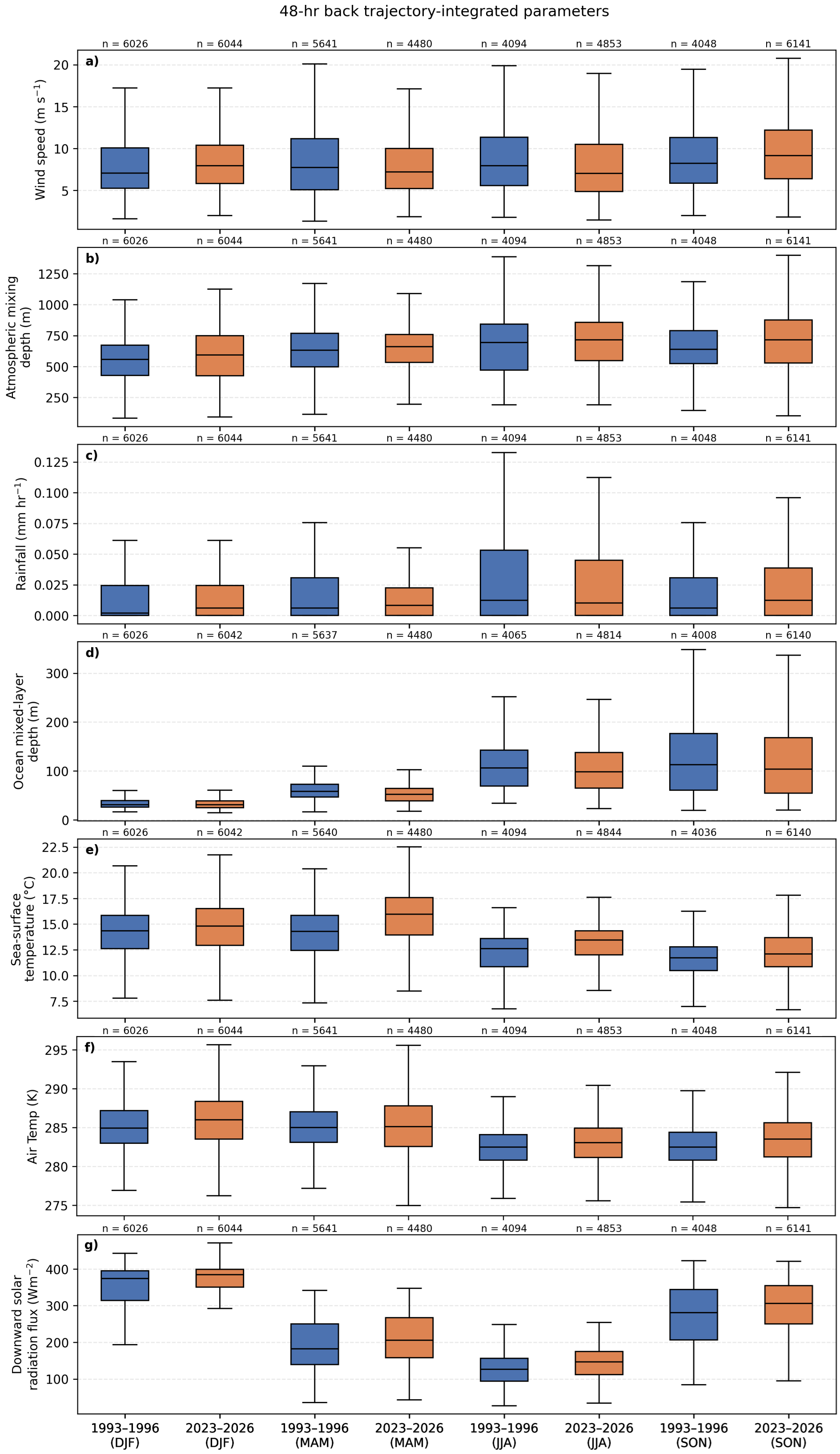

Fig. S8 Comparison of seasonal distributions of 48-h HYSPLIT back-trajectory-integrated parameters between the historical (1993-1996) and recent (2023-2026) periods. Panels show (a) wind speed (derived from the Haversine distance between consecutive trajectory locations divided by the 1-h time interval), (b) mean atmospheric mixing depth, (c) mean rainfall, (d) mean ocean mixed-layer depth, (e) mean sea-surface temperature, (f) air temperature, and (g) mean downward solar radiation flux averaged along each trajectory. Boxplots show the median (horizontal line), IQR (box), and whiskers extending to 1.5 × IQR, with outliers excluded. The number of trajectories contributing to each distribution is indicated above each boxplot.

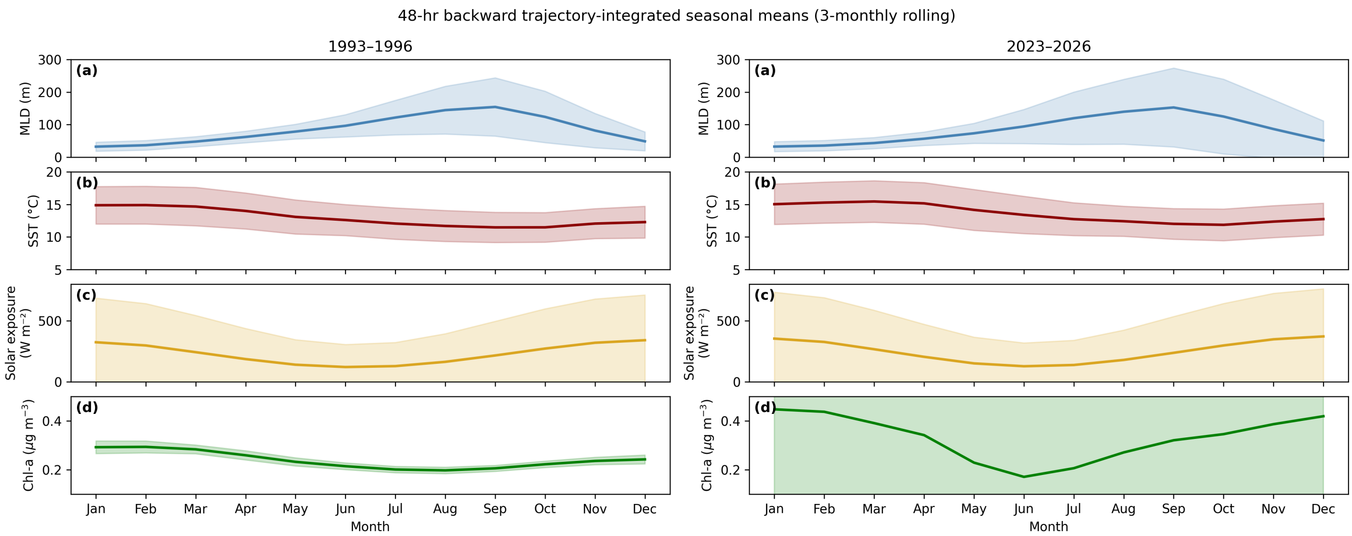

Fig. S9 Seasonal cycles of mean 48-h back trajectory-integrated variables for the historical (1993–1996; left column) and recent (2023–2026; right column) periods. Panels show monthly mean (a) ocean mixed-layer depth (MLD), (b) sea-surface temperature (SST), (c) downward solar radiation flux, and (d) chlorophyll-a. Solid lines denote centred 3-month rolling averages of the monthly means, while shaded regions represent ±1 standard deviation.

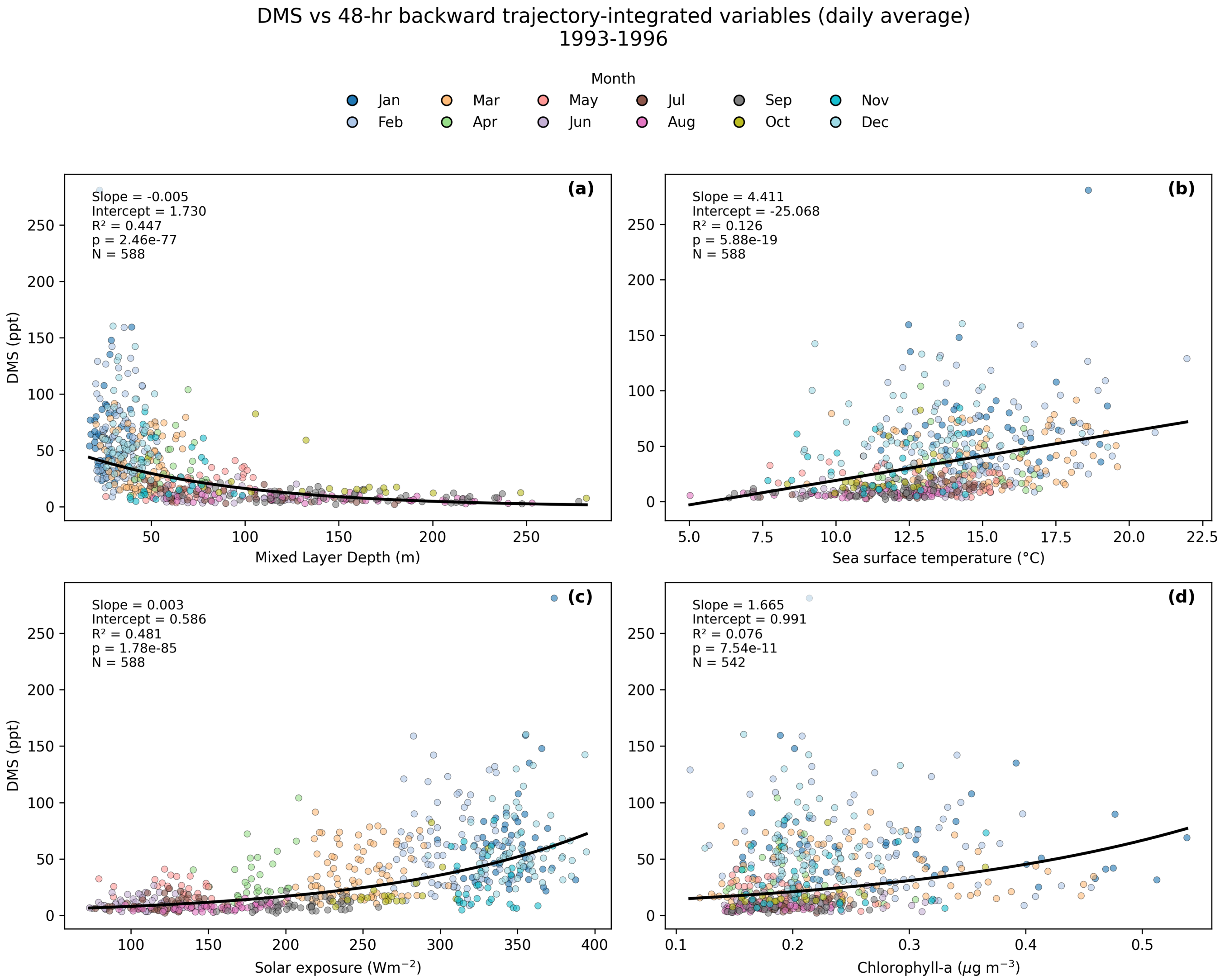

Fig. S10 Relationships between daily mean 48-h back-trajectory-integrated variables and atmospheric DMS concentrations in the 1990s dataset. Scatterplots show DMS concentrations as a function of (a) ocean mixed-layer depth (MLD), (b) sea-surface temperature (SST), (c) downward solar radiation flux, and (d) chlorophyll-a concentration. Individual points represent daily averages calculated from trajectory-integrated observations, with colours indicating the month of occurrence. Solid black lines show linear regressions fitted to the daily observations.

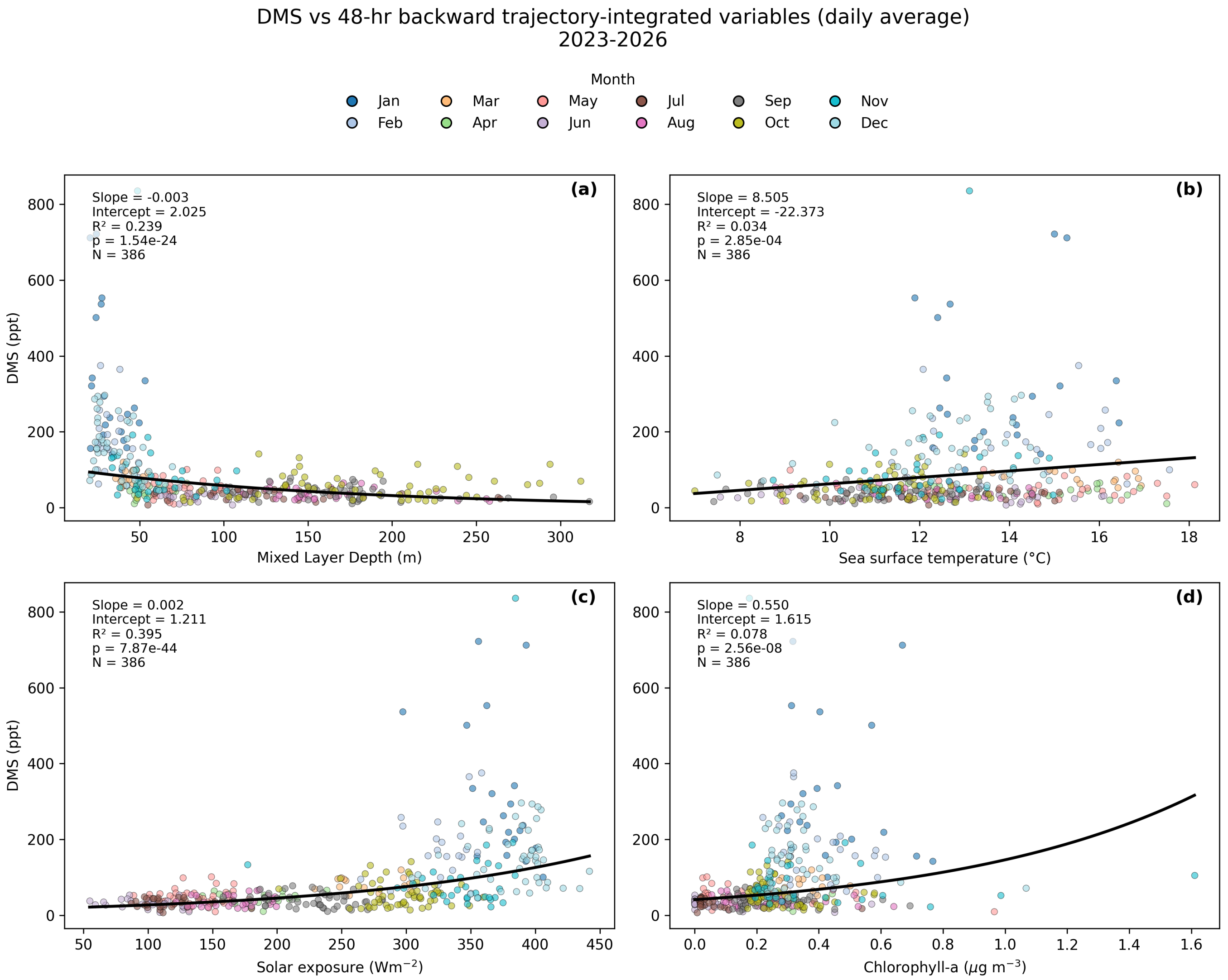

Fig. S11 Relationships between daily mean 48-h back-trajectory-integrated variables and atmospheric DMS concentrations in the 2020s dataset. Scatterplots show DMS concentrations as a function of (a) ocean mixed-layer depth (MLD), (b) sea-surface temperature (SST), (c) downward solar radiation flux, and (d) chlorophyll-a concentration. Individual points represent daily averages calculated from trajectory-integrated observations, with colours indicating the month of occurrence. Solid black lines show linear regressions fitted to the daily observations.

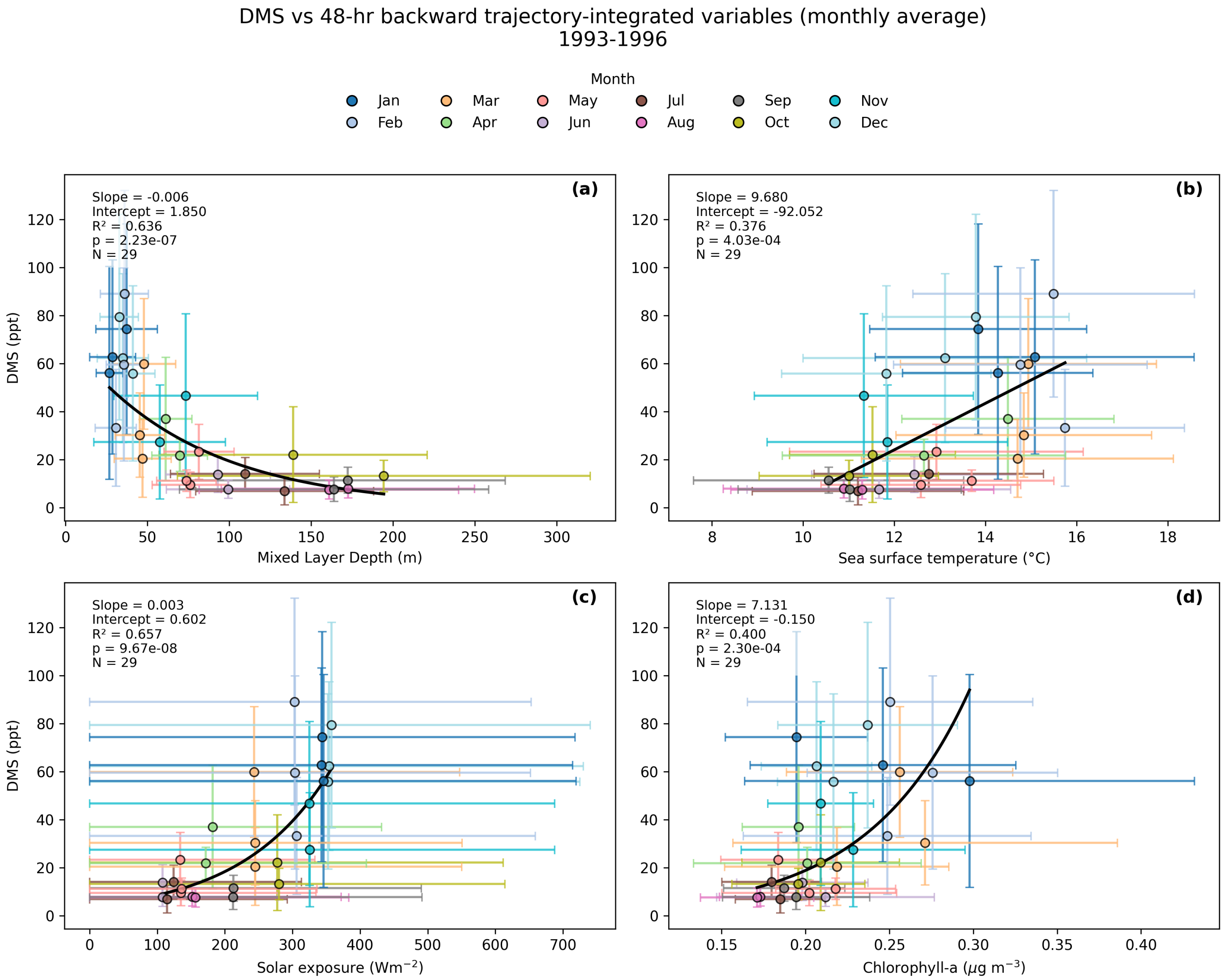

Fig. S12 Relationships between monthly mean 48-h back-trajectory-integrated variables and atmospheric DMS concentrations in the 1990s dataset. Each point represents a year-month mean with error bars showing ±1 standard deviation of the corresponding monthly observations. Panels show relationships between DMS concentration and (a) ocean mixed-layer depth (MLD), (b) sea-surface temperature (SST), (c) downward solar radiation flux, and (d) chlorophyll-a concentration.

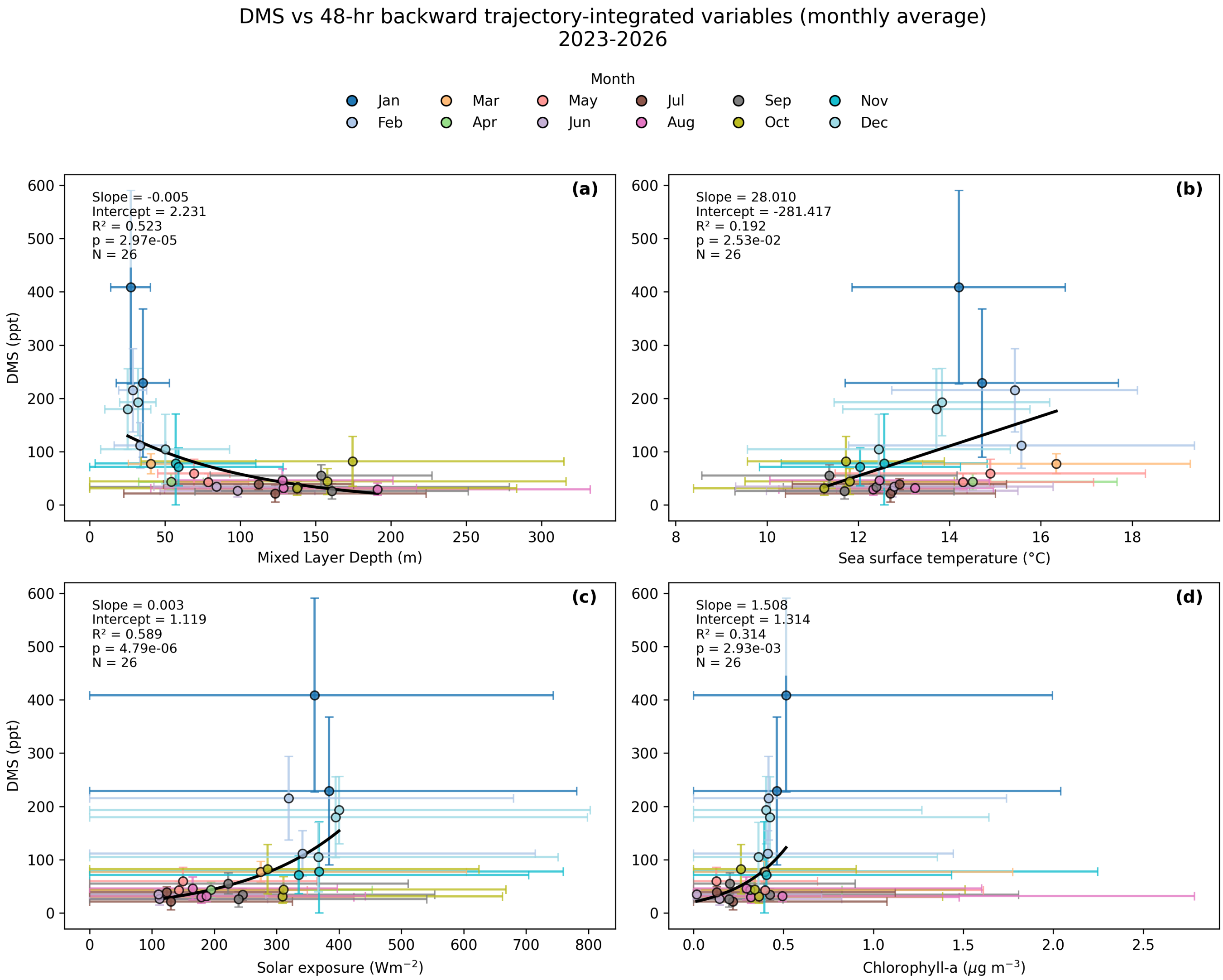

Fig. S13 Relationships between monthly mean 48-h back-trajectory-integrated variables and atmospheric DMS concentrations in the 2020s dataset. Each point represents a year-month mean with error bars showing ±1 standard deviation of the corresponding monthly observations. Panels show relationships between DMS concentration and (a) ocean mixed-layer depth (MLD), (b) sea-surface temperature (SST), (c) downward solar radiation flux, and (d) chlorophyll-a concentration.

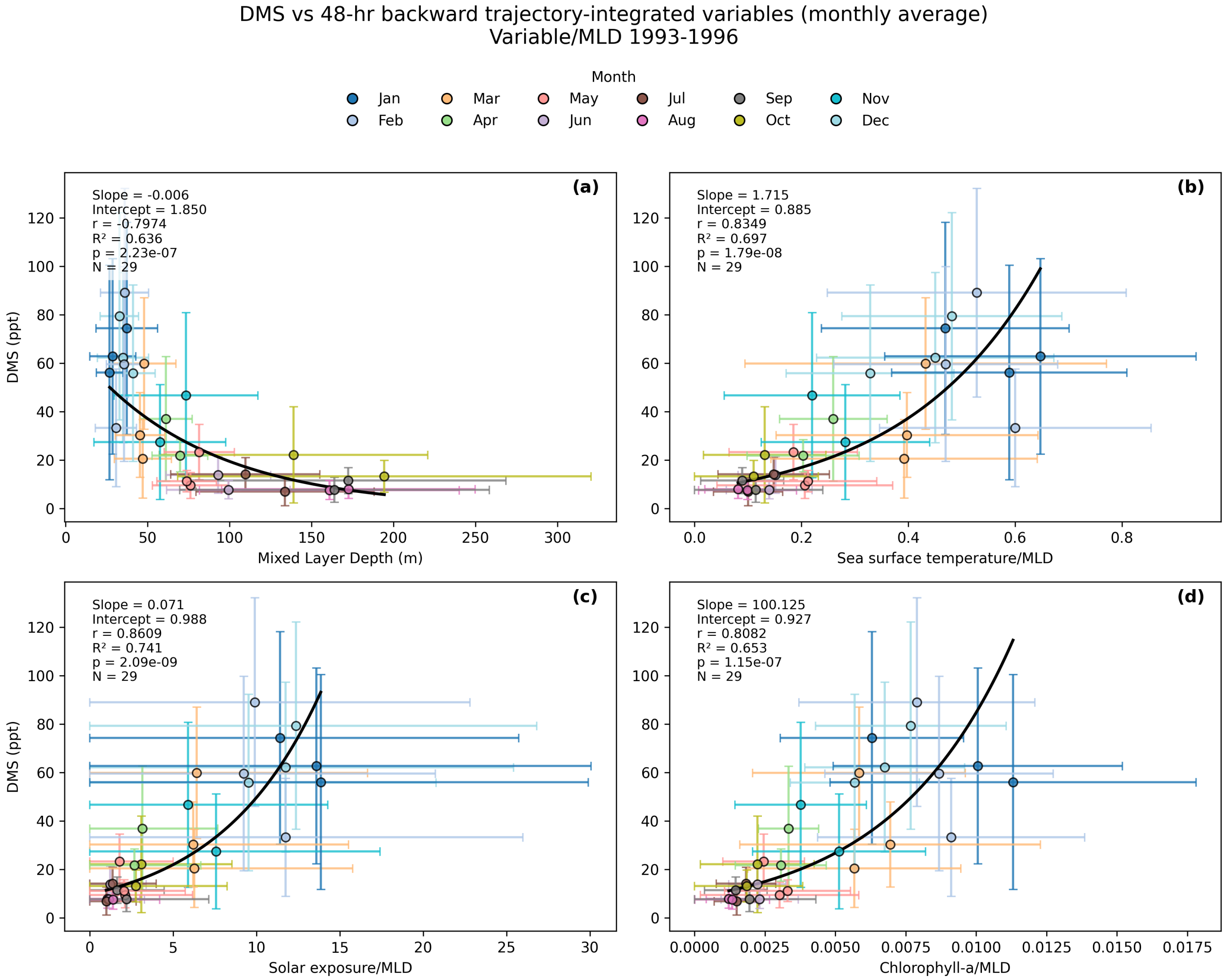

Fig. S14 Relationships between mixed-layer-depth-normalized monthly mean 48-h back-trajectory-integrated variables and atmospheric DMS concentrations in the 1990s dataset. Each point represents a year–month mean derived from 48-h back-trajectory-integrated observations, with error bars indicating ±1 standard deviation within each year–month period. Panels show DMS relationships with (a) ocean mixed-layer depth (MLD), (b) sea-surface temperature normalized by MLD (SST/MLD), (c) solar radiation exposure normalized by MLD (solar exposure/MLD), and (d) chlorophyll-a concentration normalized by MLD (chlorophyll-a/MLD).

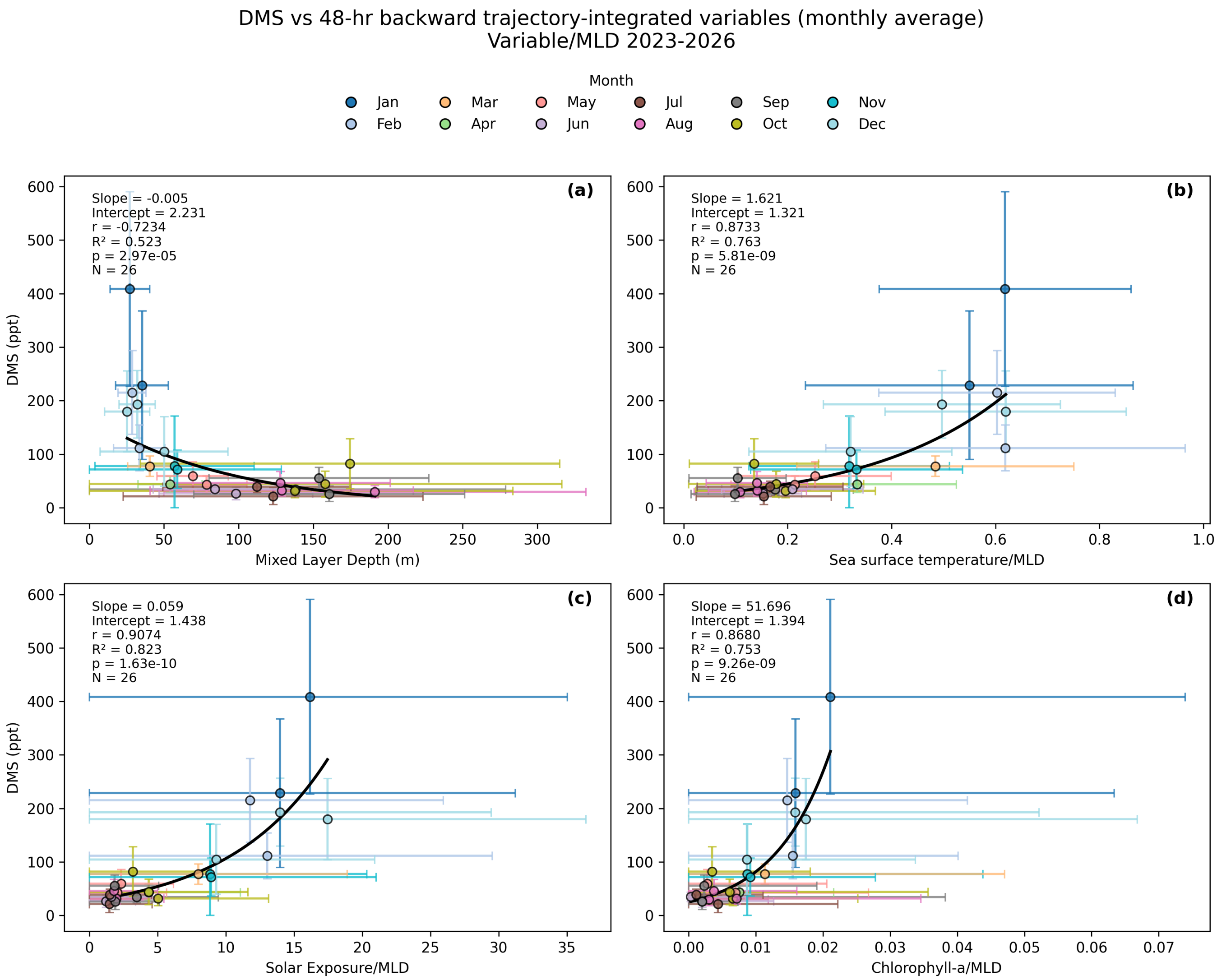

Fig. S15 Relationships between mixed-layer-depth-normalized monthly mean 48-h back-trajectory-integrated variables and atmospheric DMS concentrations in the 2020s dataset. Each point represents a year–month mean derived from 48-h back-trajectory-integrated observations, with error bars indicating ±1 standard deviation within each year–month period. Panels show DMS relationships with (a) ocean mixed-layer depth (MLD), (b) sea-surface temperature normalized by MLD (SST/MLD), (c) solar radiation exposure normalized by MLD (solar exposure/MLD), and (d) chlorophyll-a concentration normalized by MLD (chlorophyll-a/MLD).

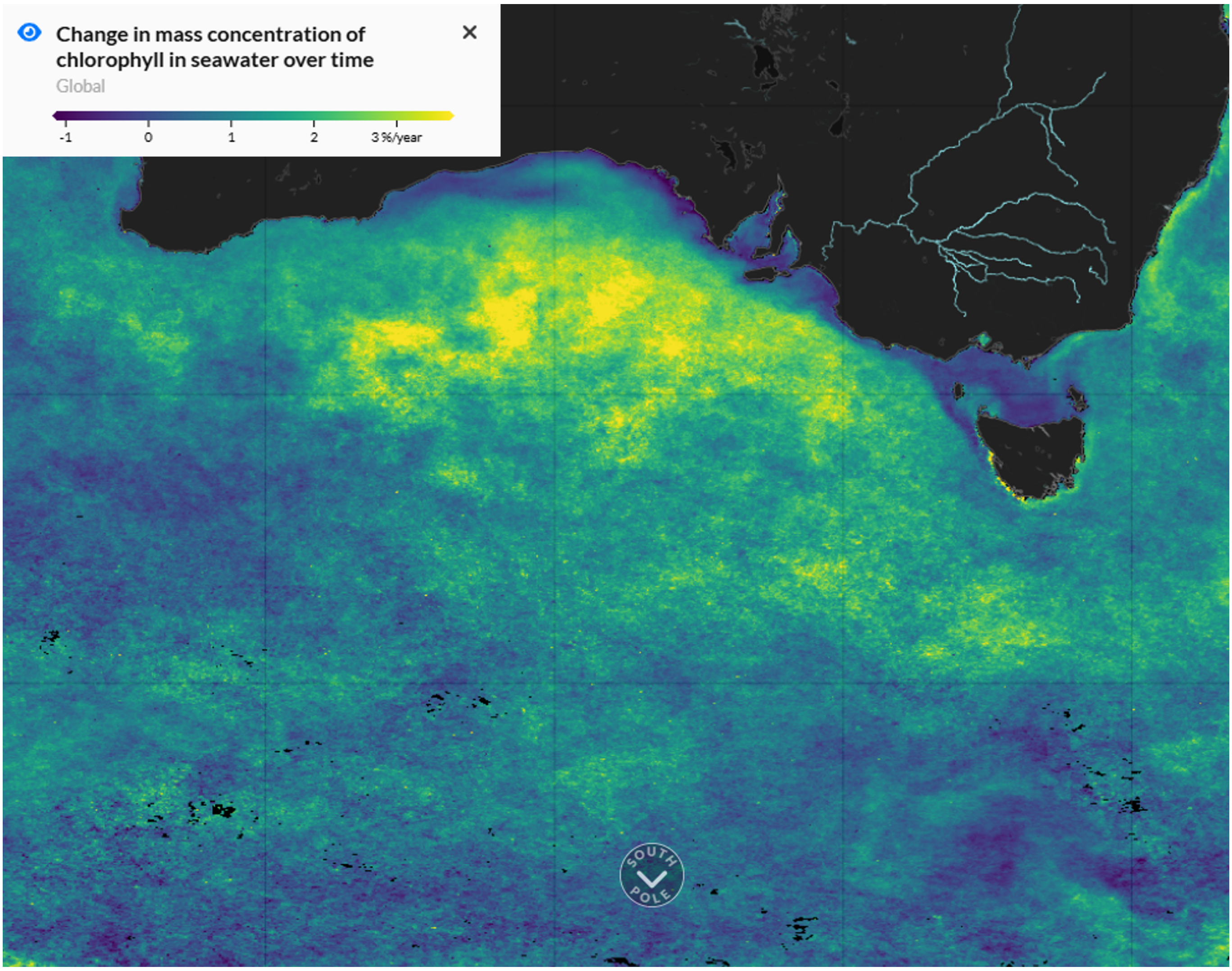

Fig. S16 Satellite chlorophyll-a trend over the period 1997-2021 based on the CMEMS multi-sensor satellite observations from product OCEANCOLOR_GLO_BGC_L4_MY_009_108 . The trend is expressed in % change in chlorophyll-a per year with positive trends in green/yellow and negative trends in dark blue/purple. Credit: E.U. Copernicus Marine Service Information.

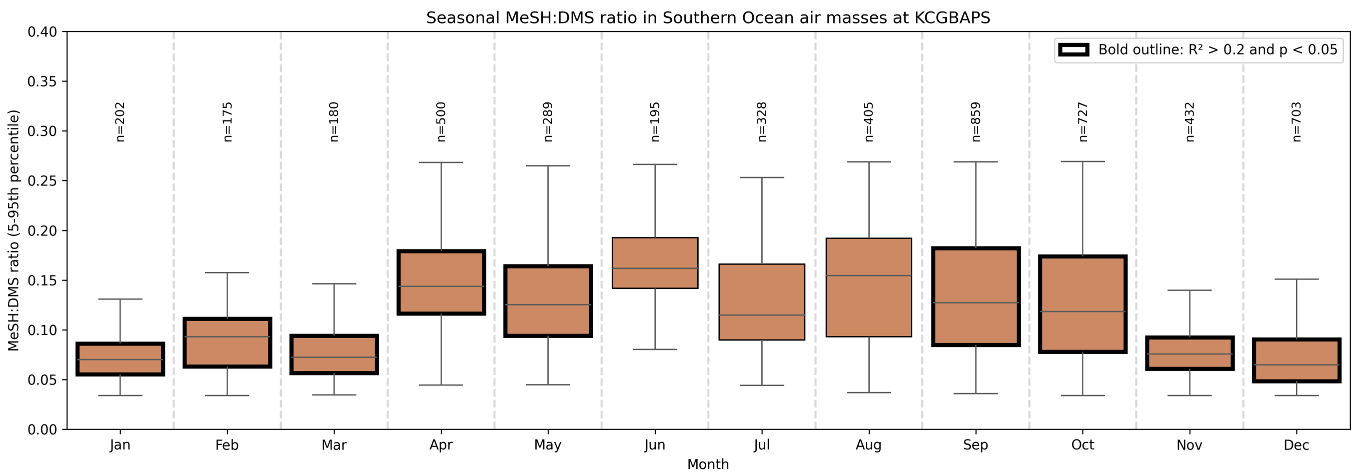

Fig. S17 Seasonal cycle of the atmospheric MeSH:DMS ratio observed at Kennaook-Cape Grim (2023–2026). The MeSH:DMS ratio was calculated from 30-min median atmospheric MeSH and DMS concentrations. Extreme ratios outside the 5th-95th percentile range of the full distribution were excluded prior to historical MeSH reconstruction in the main text. Boxplots show monthly medians and interquartile ranges, with whiskers extending to 1.5× the interquartile range and n indicating the number of 30-min observations retained per month. Bold outlines on boxplots indicate that the averages of monthly RMA regressions of MeSH vs. DMS across 2023-26 were $R^2 > 0.2$ and $p < 0.05$.

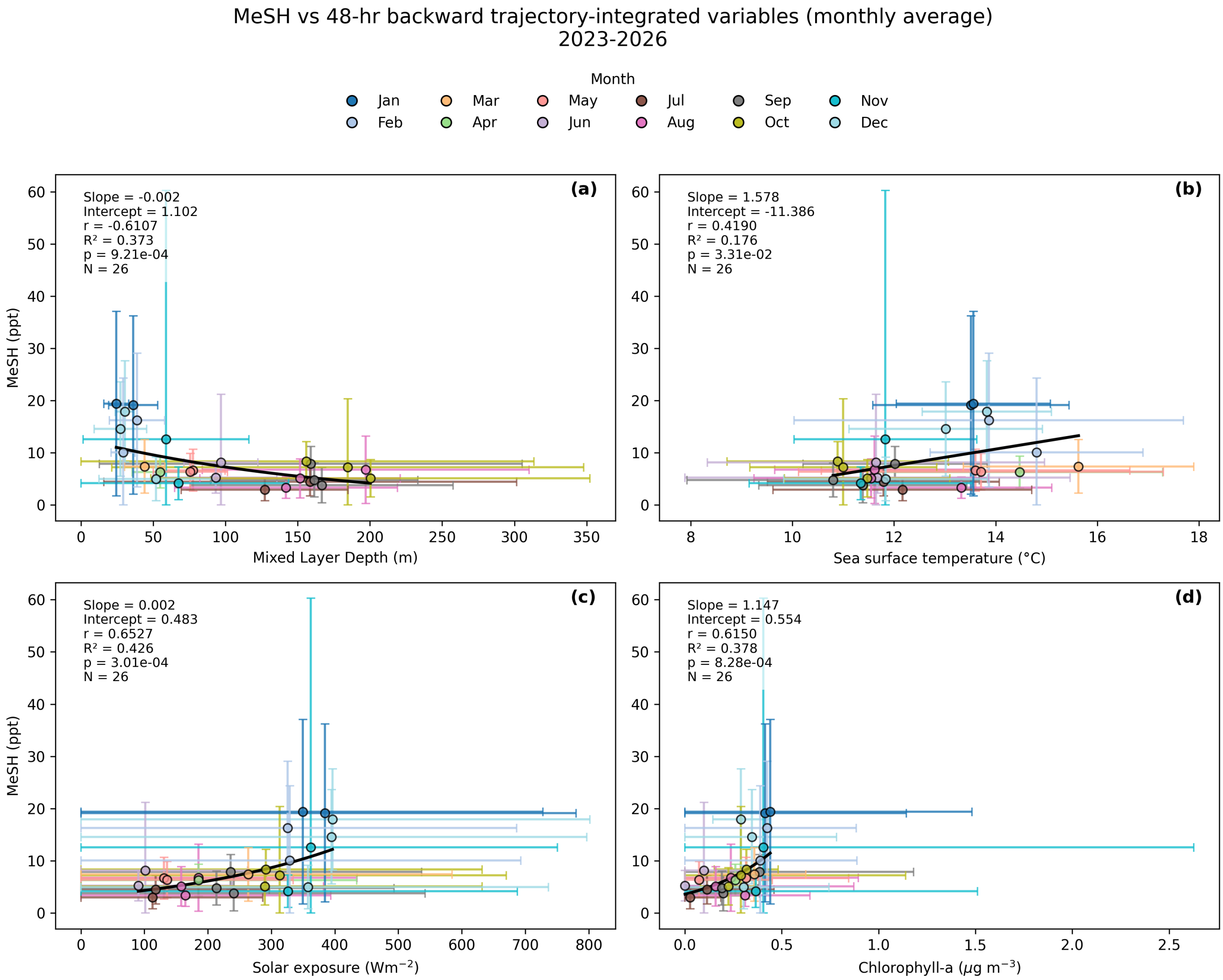

Fig. S18 Relationships between monthly mean 48-h back-trajectory-integrated variables and atmospheric MeSH concentrations in the 2020s dataset. Each point represents a year-month mean with error bars showing ± 1 standard deviation of the corresponding monthly observations. Panels show relationships between MeSH concentration and (a) ocean mixed-layer depth (MLD), (b) sea-surface temperature (SST), (c) downward solar radiation flux, and (d) chlorophyll-a concentration.

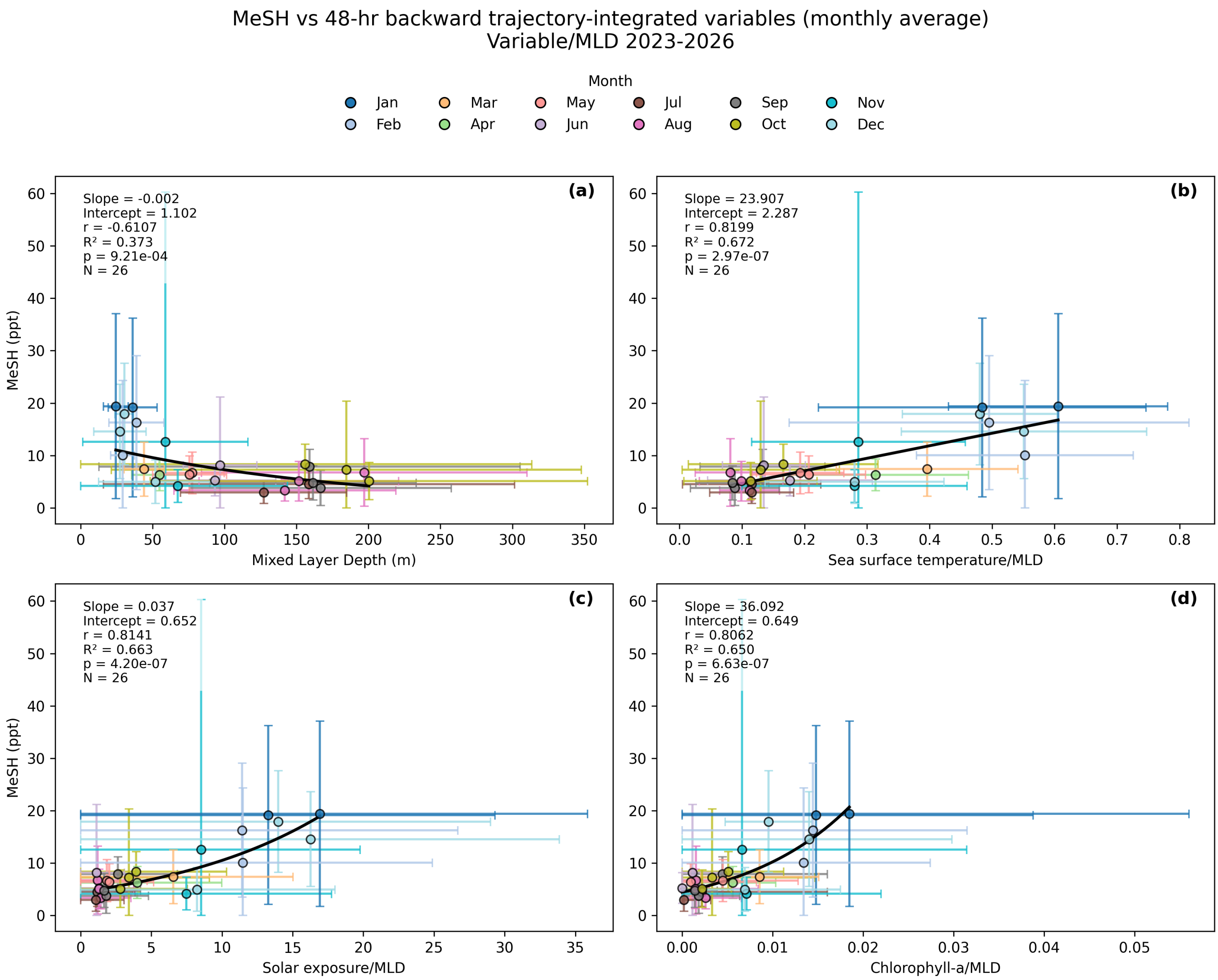

Fig. S19 Relationships between mixed-layer-depth-normalized monthly mean 48-h back-trajectory-integrated variables and atmospheric MeSH concentrations in the 2020s dataset. Each point represents a year–month mean derived from 48-h back-trajectory-integrated observations, with error bars indicating ±1 standard deviation within each year–month period. Panels show MeSH relationships with (a) ocean mixed-layer depth (MLD), (b) sea-surface temperature normalized by MLD (SST/MLD), (c) solar radiation exposure normalized by MLD (solar exposure/MLD), and (d) chlorophyll-a concentration normalized by MLD (chlorophyll-a/MLD).

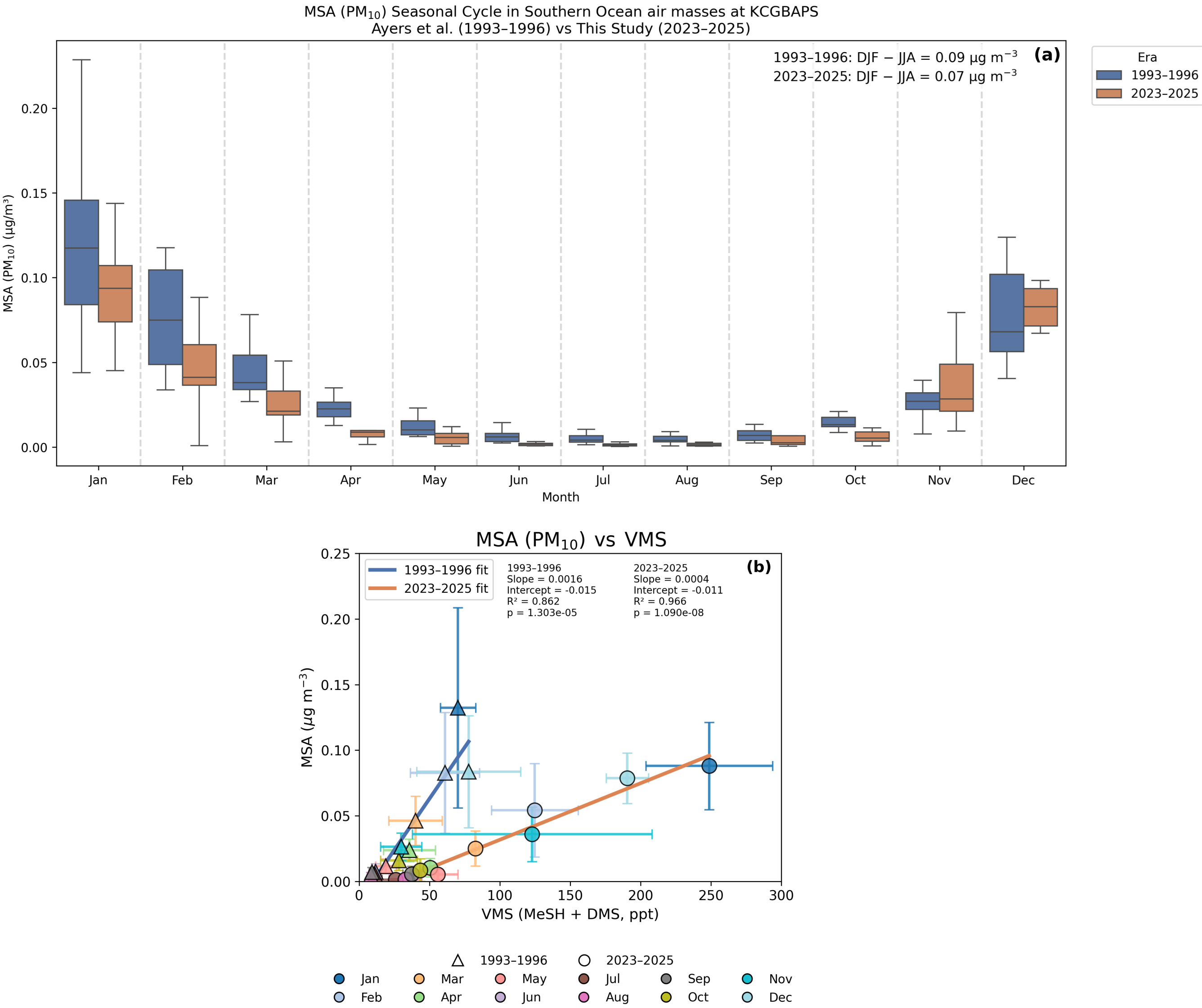

Fig. S20 (a) Seasonal cycle of PM_{10} methanesulfonic acid (MSA) concentrations comparing historical observations 1993–1996 (blue) with measurements from the present study 2023–2025 (orange; data were only available until May 2025). (b) Relationship between VMS_a (using 2023-2025 observations of DMS and MeSH, and interpolated MeSH observations for 1993-1996) and PM_{10} MSA concentrations.

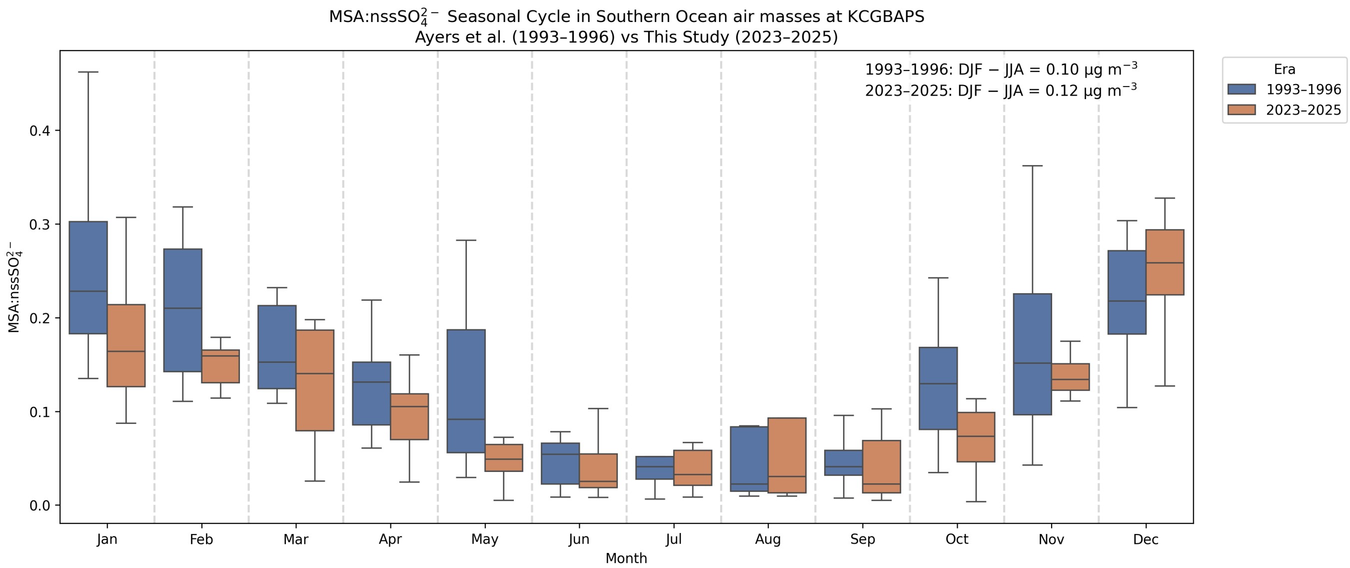

Fig. S21 Seasonal cycle of PM_{10} MSA:nssSO_4^{2-} concentrations comparing historical observations 1993–1996 (blue) with measurements from the present study 2023–2025 (orange; data were only available until May 2025).

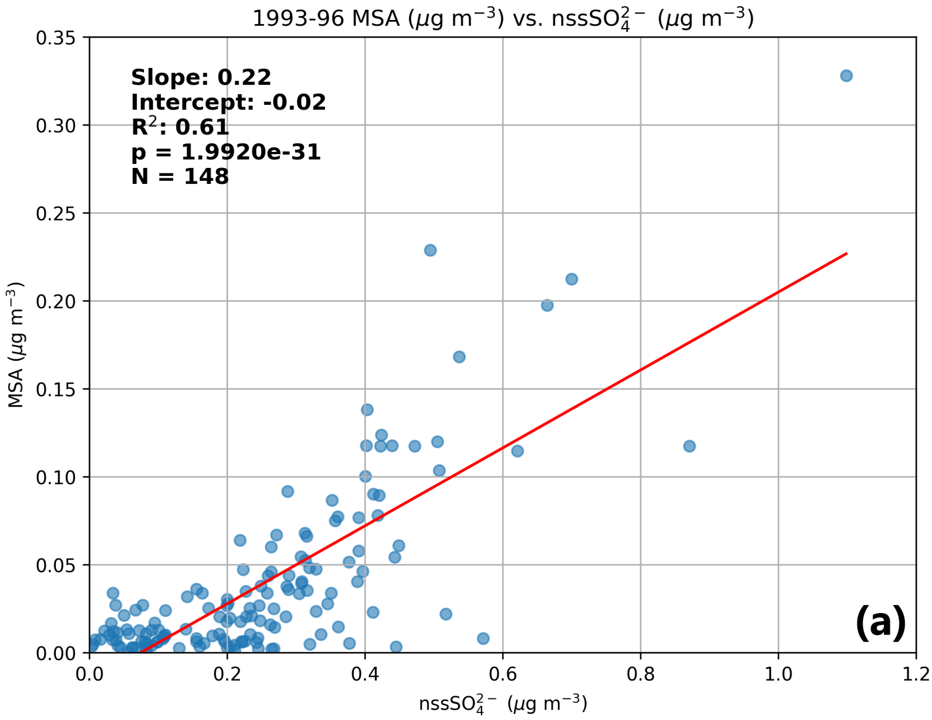

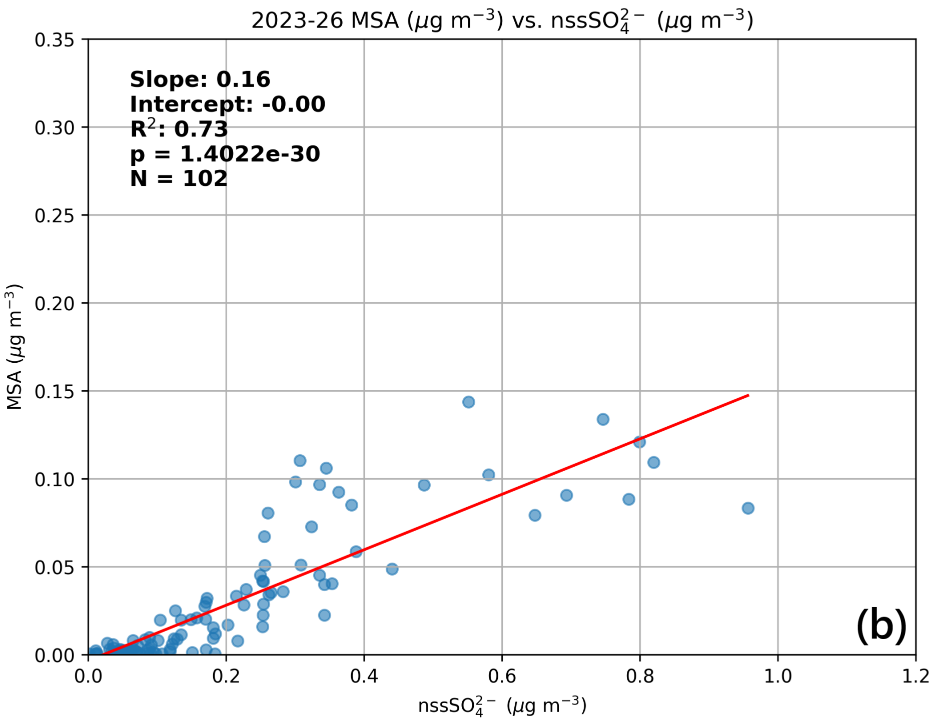

Fig. S22 Relationship between PM_{10} MSA and PM_{10} nssSO_4^{2-} concentrations.

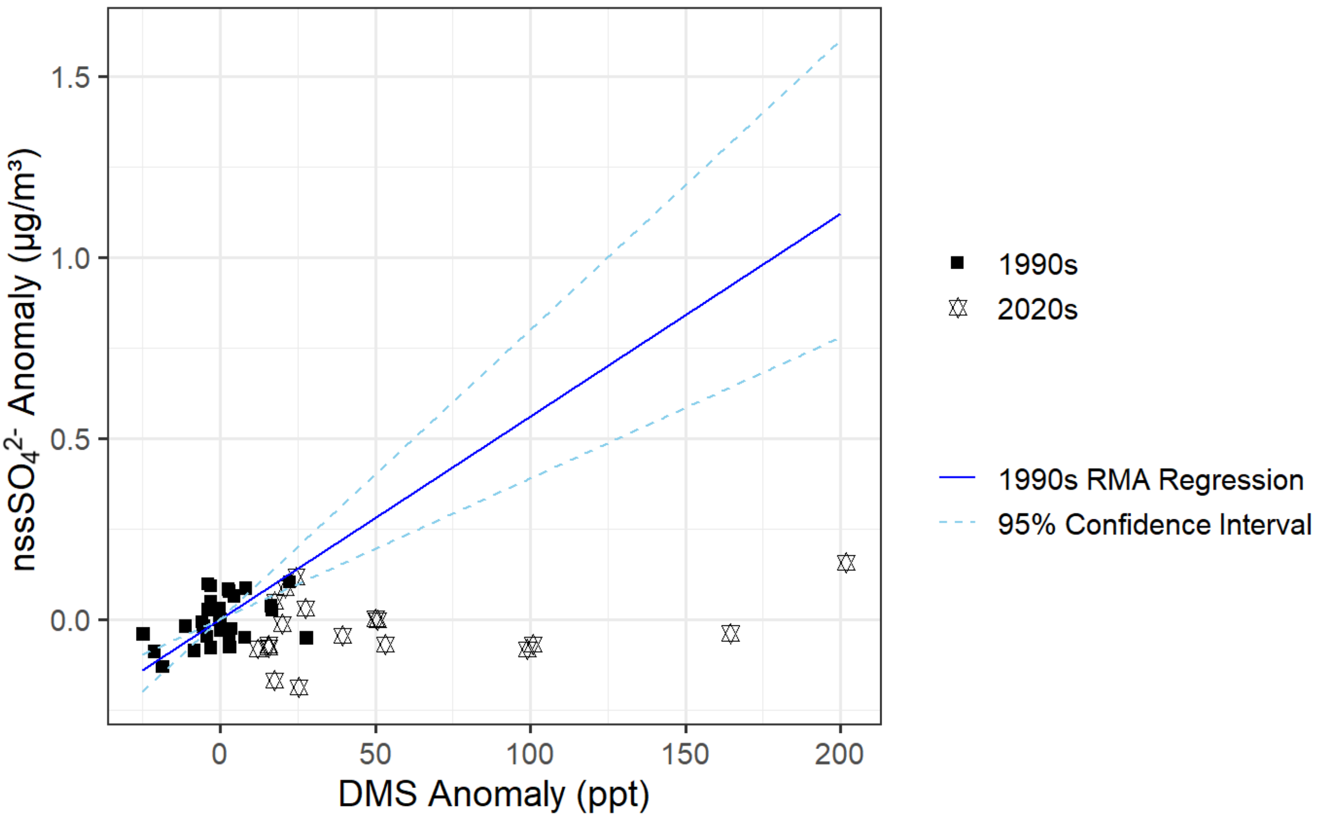

Fig. S23 Relationship between monthly PM_{10} non-sea-salt sulfate and DMS anomalies. Monthly mean concentrations were aggregated by month and year, with anomalies calculated relative to the corresponding calendar-month conditions across the 1990s. Each point therefore represents the departure from the typical concentration for that month. Squares denote 1990s observations and stars denote 2020s observations. The solid blue line shows the reduced major axis (RMA) regression and the dashed light blue lines show the 95 % confidence interval of slopes from the RMA regression analysis.

References

[1] Ayers, G.P., Gillett, R.W.: DMS and its oxidation products in the remote marine atmosphere: Implications for climate and atmospheric chemistry. Journal of Sea Research **43**(3-4), 275–286 (2000) https://doi.org/10.1016/S1385-1101(00)00022-8 . Issue: 3-4

[2] Andreae, M.O., Ferek, R.J., Bermond, F., Byrd, K.P., Engstrom, R.T., Hardin, S., Houmere, P.D., LeMarrec, F., Raemdonck, H., Chatfield, R.B.: Dimethyl sulfide in the marine atmosphere. Journal of Geophysical Research: Atmospheres **90**(D7), 12891–12900 (1985) https://doi.org/10.1029/JD090iD07p12891 . Accessed 2026-08-02

[3] Berresheim, H., Andreae, M.O., Ayers, G.P., Gillett, R.W., Merrill, J.T., Davis, V.J., Chameides, W.L.: Airborne measurements of dimethylsulfide, sulfur dioxide, and aerosol ions over the Southern Ocean South of Australia. Journal of Atmospheric Chemistry **10**(3), 341–370 (1990) https://doi.org/10.1007/BF00053868 . Publisher: Springer. Accessed 2026-08-02

[4] Ayers, G.P., Bentley, S.T., Ivey, J.P., Forgan, B.W.: Dimethylsulfide in marine air at Cape Grim, 41°S. Journal of Geophysical Research: Atmospheres **100**(D10), 21013–21021 (1995) https://doi.org/10.1029/95JD02144 . Accessed 2025-07-11

[5] Sciare, J., Mihalopoulos, N., Nguyen, B.C.: Summertime Seawater Concentrations of Dimethylsulfide in the Western Indian Ocean: Reconciliation of Fluxes and Spatial Variability with Long-Term Atmospheric Observations. Journal of Atmospheric Chemistry **32**(3), 357–373 (1999) https://doi.org/10.1023/A:1006132001945 . Publisher: Springer. Accessed 2026-08-03

[6] Bruyn, W.J., Harvey, M., Cainey, J.M., Saltzman, E.S.: DMS and SO2 at Baring Head, New Zealand: Implications for the Yield of SO2 from DMS. Journal of Atmospheric Chemistry **41**(2), 189–209 (2002) https://doi.org/10.1023/A:1014252106572 . Accessed 2024-10-06

[7] Colomb, A., Gros, V., Alvain, S., Sarda-Esteve, R., Bonsang, B., Moulin, C., Klüpfel, T., Williams, J.: Variation of atmospheric volatile organic compounds over the Southern Indian Ocean (30 - 49°S). Environmental Chemistry **6**(1), 70 (2009) https://doi.org/10.1071/EN08072 . Accessed 2023-12-05

[8] Galbally, I.E., Lawson, S.J., Weeks, I.A., Bentley, S.T., Gillett, R.W., Meyer, M., Goldstein, A.H.: Volatile organic compounds in marine air at Cape Grim, Australia. Environmental Chemistry **4**(3), 178–182 (2007) https://doi.org/10.1071/EN07024

[9] Lawson, S.J., Law, C.S., Harvey, M.J., Bell, T.G., Walker, C.F., De Bruyn, W.J., Saltzman, E.S.: Methanethiol, dimethyl sulfide and acetone over biologically productive waters in the southwest Pacific Ocean. Atmospheric Chemistry and Physics **20**(5), 3061–3078 (2020) https://doi.org/10.5194/acp-20-3061-2020 . Publisher: Copernicus GmbH

[10] Dunne, E., Humphries, R., Mynard, C., McRobert, I., Harnwell, J., Cravigan, L., Lawson, Sarah (CSIRO): CAPRICORN - Atmospheric VOC measurements from the RV Investigator voyage IN2016_V02 [Dataset]. CSIRO Data Collection (2024). https://doi.org/10.25919/574m-7e47

[11] Rocco, M., Dunne, E., Salignat, R., Saint-Macary, A., Peltola, M., Barthelmeß, T., Chamba, G., Barr, N., Safi, K., Marriner, A., Deppeler, S., Rose, C., Uitz, J., Harnwell, J., Engel, A., Colomb, A., Saiz-Lopez, A., Harvey, M.J., Law, C.S., Sellegri, K.: Relating Dimethyl Sulphide and Methanethiol Fluxes to Surface Biota in the South-West Pacific Using Shipboard Air-Sea Interface Tanks. Journal of Geophysical Research: Atmospheres **130**(1), 2024–041072 (2025) https://doi.org/10.1029/2024JD041072 . Accessed 2025-01-08

[12] Mynard, C., Franklin, E.B., Alroe, J., Somerville, N., Patti, A., Siems, S.T., Williams, A., Mallet, M.D., Humphries, R., Dunne, E.: Constraining Atmospheric Methanethiol Estimates Over the Southern Ocean. Geophysical Research Letters **52**(18), 2025–116470 (2025) https://doi.org/10.1029/2025GL116470 . Accessed 2025-09-15

[13] Derek, N., Krummel, P.: Baseline Atmospheric Program Australia 2007-2008 (2011) https://doi.org/10.25919/5F2075C5E2EC5 . Accessed 2024-05-07

[14] NASA Earth Observations: Chlorophyll Concentration (1 month - Aqua/MODIS) | NASA [Dataset]. Publisher: NASA Earth Observations (NEO) (2025). https://neo.gsfc.nasa.gov/view.php?datasetId=MY1DMM_CHLORA&date=2024-01-17 Accessed 2025-02-20